ISSN 1392 - 1207. MECHANIKA. 2013 Volume 19(4): 451-458

Segmentation of piezoelectric layers based on the numerical study of normal strain distributions in bimorph cantilevers vibrating in the second transverse mode

D. Žižys, R. Gaidys, R. Daukševičius, V. Ostaševičius
Kaunas University of Technology, Kęstučio 27, 44312 Kaunas, Lithuania, E-mail: Rimvydas.Gaidys@ktu.lt

crossref http://dx.doi.org/10.5755/j01.mech.19.4.4477

1. Introduction

Nowadays energy harvesting is becoming an increasingly important issue for low-power micro-systems (for e.g. wireless node systems, seismic sensors, etc.). Progress in modern ultra-low-power microelectronics demand a promote progress in micro-energy harvesting from ambient energy sources to create self-powered microsystems. Since usual locations for such systems are hardly accessible it is natural that it is required that these sensors or systems would be self-powered, would satisfy certain size and mass requirements, and would assure continuous, long-term, uninterrupted power supply without replacement of batteries or other elements. Several ambient energy sources could be harnessed for this purpose such as thermal gradients, photonic energy, various forms of radiation though the biggest potential is seen in mechanical energy and vibrational energy in particular since low and medium frequency vibrations are all around us and may offer a constant and reliable power supply if harnessed correctly. During recent years energy harvesting from vibration sources has attracted a lot of interest, particularly as micro energy sources. The main application for these are wireless sensor nodes, communication modules, etc. Supply powers of < 100 μW are sufficient to operate wireless nodes in silent mode. The duty cycle can be quite small so that mW supply levels already enable some autonomy. Motion and vibrations are the most versatile and ubiquitous ambient energy source available [1]. The mechanical to electrical energy transformation is most efficiently done by piezoelectric materials [2].

Among numerous advantages of vibration energy harvesting there are some drawbacks too. The most significant of those is their low efficiency and the fact that their maximum power output is reached only when the frequency of ambient vibrations matches the resonant frequency of the harvester device. When the vibration of the environment passes resonant frequency of the harvesters its efficiency drops significantly. There are numerous solutions offered to overcome these drawbacks such as widening the broadband frequency of the harvesters by changing the shape, mass or parameters of the harvesters or introducing arrays of different harvesters for harvesting different resonant frequencies.

The paper focuses on increasing the efficiency of rectangular and optimal shape of the second and third mode transverse vibration cantilever harvesters by optimal segmentation of the piezoelectric materials of different polarization on the face of the cantilever. To utilize this goal the rectangular cantilever is investigated at its second resonant frequency of 541 Hz at settled vibration state as well as two optimal shape cantilevers at their second resonant frequency of 534 Hz. The optimal shape cantilever means that the cantilever is designed to match the rectangular cantilevers resonant frequency (second and third resonant frequencies in this case) but to have minimal mass. The normal strain along the length of cantilever is assumed to be directly proportional to the power output of the piezoelectric layer of corresponding sign. The results are assumed to be universal for any cantilever harvester of such type. Fig. 1 illustrates the distribution of utilization of different vibration frequencies and accelerations by different kinds of vibrational energy harvesters.

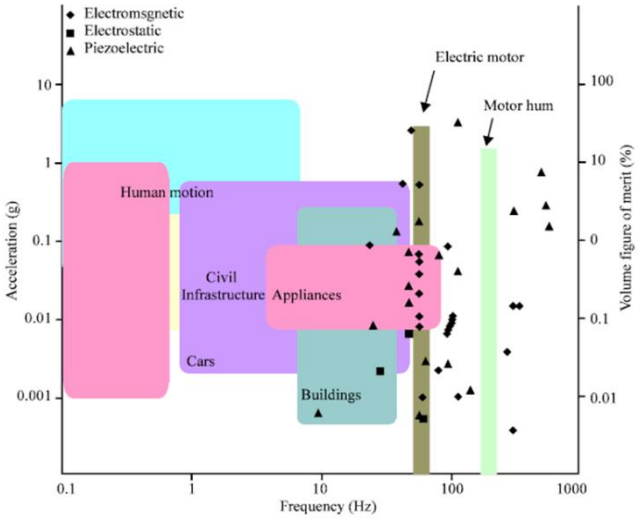

Fig. 1 Distribution of utilization of different vibration frequencies and accelerations by different kinds of vibrational energy harvesters [1]

1.1. Cantilever type harvester setup

Various forms and shapes of the cantilevers have been proposed to increase the power output from strains in cantilver type generators. Glynne-Jones proposed and modeled a tapered beam generator. The tapered beam setup is different from normal rectangular cantilever harvester that the constant strain is assured along the whole length of the cantilver for given displacements. The device was manufactured from 0.1 mm thick AISI 316 stainless steel. The piezoelectric material used was PZT-5H powder mixed with Corning 7575 glass and a suitable thick-film vehicle to form a screen printable thixotropic paste. Both faces of the cantilever were coated to cancel the uneven thermal expansion of the cantilever and to maximize the

power output. The structure was excited at its first natural resonant frequency of 80.1 Hz and generated 3 μW at 333 kΩ [2].

There is also wide range of active materials to choose since the deposition techniques are well developed for both thin and thick films [3]. This was a constant width steel bar with two layers of PZT-5A on top and bottom of the bar. The drawback of this design was that the strain was distributed unequally along the bar; the mathematical models describing this phenomenon are presented in [4]. A cubic mass made of tin and bismuth composite was attached on the tip of the cantilever. The designed resonant frequency for the structure was 120 Hz. The maximum output value reached was 80 μW into a 250 kΩ load resistance with 2.5 m/s^2 input acceleration and the results showed a reasonable level of agreement with the analytical models. Using these models as reference the structure was optimized to overall size constraint of 1 cm^3. Two further designs were developed, each using two PZT-5H layers attached to a 0.1 mm central brass. The paper [5] provides results of dynamic numerical analysis of piezoelectric cantilever-type microgenerator intended for wireless MEMS applications. This analysis constitutes an initial phase of ongoing research work aimed at microgenerator optimal design. It is based on beneficial utilization of higher vibration modes, which may offer significant benefits in terms of dynamic performance. Here we report preliminary results of simulations that were performed with a developed 3D finite element model of the microgenerator that constitutes a bilayer cantilever structure with proof mass at the free end. The structure was subjected to harmonic base excitation by applying vertical acceleration through body load. The resulting characteristics reveal strong dependence of magnitude of generated voltage on design and excitation parameters (frequency, acceleration). Initial findings indicate the necessity to develop microgenerator design with self-tuning of the resonance frequency, i.e. the device should adapt to varying excitation frequency so as to be driven in resonance thereby achieving maximal electrical power output. Paper [6] reports on numerical modeling and simulation of a generalized contact-type MEMS device having large potential in various microsensor/actuator applications, which are currently limited because of detrimental effects of the contact bounce phenomenon that is still not fully explained and requires comprehensive treatment. The proposed 2D finite element model encompasses cantilever microstructures operating in a vacuum and impacting on a viscoelastic support. The presented numerical analysis focuses on the first three flexural vibration modes and their influence on dynamic characteristics. Simulation results demonstrate the possibility to use higher modes and their particular points for enhancing MEMS performance and reliability through reduction of vibro-impact process duration. In [7] a piezoelectric generator composed from a beam and a proof mass of is designed and installed on a bicycle handlebar; the first experiments have shown that the few mW that produced the piezoelectric generator is able to power LED-lamp. Under ideal conditions such as pure sinusoidal vibrations at 5 ms^2 and 12.5 Hz, the power harvestable measured achieved 3.5 mW for an optimal resistive load of 100 kW, power that is sufficient to recharge a battery, or to power low consumption devices.

These types of generators are the simplest while the mechanical motion is directly converted into a voltage output via electrode active material. This type of device can be used for both impact and vibration energy harvesting without need for numerous additional components. This type of generators is particularly well suited for micro-engineering. On the other hand PZT is known to provide high output voltage but low output currents. The piezoelectric materials are required to be strained directly and therefore their mechanical properties will limit the overall performance and lifetime. Also the transduction efficiency is ultimately limited by piezoelectric properties of materials employed. The output impedance of piezoelectric generators is typically very high (> 100 kΩ) [8].

These and other sources were used to analyze the normal strain distribution in direction along of the cantilever. Normal strain is analyzed because there is a direct relation between normal strains appearing on the face of the cantilever and thus in the layer of piezoelectric material, and energy output of piezoelectric material placed on that cantilever. Measuring and understanding the dynamic effects appearing in the cantilever will help to optimize the energy output from these strains.

Segmentation of the piezoelectric material on the face of the cantilever is extremely important if the cantilever is going to be used at its second or higher resonant frequency since at the regions of nodes areas of uncertainty appear, where strains of both negative and positive sign appear at the same moment and thus it is important to place the piezoelectric materials of different polarizations so that the maximum of the strains would be harnessed.

In normal conditions one would segment the piezoelectric material at the middle of such region, but in this paper optimization of such regions will be done and strain, or energy output gain of such optimization will be calculated.

The objectives of this paper are to investigate normal strain distribution along length of cantilever, then the cantilever is excited at its second mode of transverse vibrations. The investigation was done for three different shape cantilevers: rectangular, optimal shape of the second mode transverse vibration and optimal shape of the third mode transverse vibration. The eigenfrequencies have the same value. After conducting the investigation optimal segmentation boundaries were calculated where tensile deformations change compression deformations and vice versa.

1.2. Derivation of characteristics

Modal analysis. Since the investigated cantilever systems are considered to be undampped that is there is no element present that is consuming the vibration energy of the cantilever the system may be considered to be undergoing free vibrations and the governing differential equation may be written as shown in (1):

$$M\ddot{u} + Ku = 0 . \quad (1)$$

Internal elastic forces Ku act as an offset to the internal forces $M\ddot{u}$. In this case K is the stiffness matrix and M is the mass matrix. Differential Eq. (1) can be reduced further to get (2) through which the eigen-frequencies or resonant frequencies are found:

$$Kv = \omega^2 Mv, \quad (2)$$

where ω_i is resonant frequency or eigen-frequency and v_i is corresponding vibration mode or eigen-mode vector. Boundary condition for this cantilever is one fixed and the other end is free. The impact of ambient forces is imitated by vertical kinematic (base) excitation of the cantilever.

Equation of motion. The second problem is finding the distribution of normal strains through the face of the cantilever under investigation. For this problem differential equation of damped forced vibration was used (3). The system was subjected to time dependent force $f(t)$, which is periodic in time:

$$M\ddot{u}(t) + C\dot{u}(t) + Ku(t) = f(t). \quad (3)$$

In this case the added C is damping matrix. The time dependent force $f(t)$ is described as cantilever body load in vertical direction and defined as force/volume using the thickness:

$$f(t) = am \sin \omega_n t, \quad (4)$$

where a is acceleration and is 1.2 m/s^2, m is mass of cantilever and ω_n is the excitation frequency, which matches the second resonant frequency of the cantilever under investigation boundary conditions [6].

1.3. Finite element method models

Finite element method (FEM) was chosen to solve these differential equations numerically.

The cantilevers under investigation are considered to be thin because they satisfy the condition that thickness of the cantilever should not be bigger than one tenth of the width of the cantilever, this is important because in thin cantilevers the shear deformations in transverse direction are neglected.

Because investigated structure is thick cantilever with no strain in the out-of-plane direction the plane strain 2D continuum application mode was used for modeling. The equation of motion (3) was solved during transient analysis. The load parameters vary dependent on the excitation frequency ω_n of time dependent force $f(t)$. The element type is quadratic Lagrange elements with second-order polynomials.

Adaptive meshing and extruded triangular mesh was used to solve these problems. COMSOL 3.5a software was used. The investigation was carried out with cantilever of three different geometries.

One rectangular cantilever, and the shape of other two cantilevers was obtained by solving the shape optimization problem with the objective to obtain the cantilever of minimal mass for a given mode of transverse eigen-frequency, second and third in this case, with constraints: state Eq. (2) and the value of its eigen-frequency ω_i must be the same as value of the corresponding rectangular cantilever eigen-frequency ω_i. Optimal shape cantilevers are presented in Fig. 2. The cantilevers have been scaled by a factor of 10 in vertical direction. Mechanical properties of the material and dynamic characteristics of cantilevers are given in Table 1.

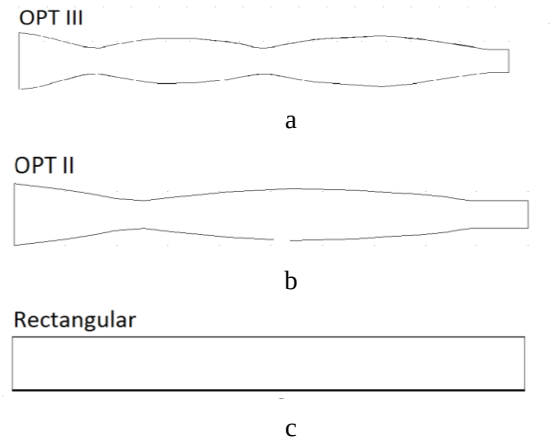

Fig. 2 Geometry of cantilever setups: a) optimal shape of the third mode transverse vibration (OPT III); b) optimal shape of the second mode transverse vibration (OPT II); c) rectangular shape (REC)

Table 1

Mechanical properties of the material and dynamic characteristics of cantilever setups

	REC	OPT II	OPT III
ω_1, Hz	86	66	66
ω_2, Hz	541	534	534
Density, kg/m^3	7850		
Elastic modulus, N/m^2	2×10^{10}		
Poisson's ratio	0.33		
Length, l	0.1 m		
Width, a	0.01 m		
Thickness, b	0.001 m for rectangular from 0.0005 m up to 0.0015 m for optimal shape		

2. Numerical analysis

Modal analysis with three different shape cantilever harvesters was performed. Results of modal analysis are presented in Table 1. From the results it can be seen that values of eigen-frequency are the same or close to it for all the cantilevers under investigation. The first vibration mode of these cantilevers in transverse direction is shown in Fig. 3 along with normal strain through the length of the cantilever, and Fig. 4 for the second vibration mode.

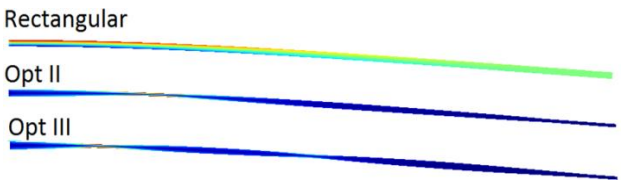

Fig. 3 The first vibration mode of three cantilever setups in transverse direction

Fig. 4 The second vibration mode of three cantilever setups in transverse direction

The bimorph rectangular cantilevers was exposed to ambient harmonic vibrations that matched their second transverse vibration resonant frequency of 541 Hz at 1.3*g* acceleration for rectangular cantilever and 534 Hz and 1.3*g* acceleration for the optimized shape cantilevers. The vertical displacement of free end of the cantilever for given interval of time can be seen in Fig. 5. From Fig. 5 it can also be observed that the interval selected for further investigation of normal strain in horizontal direction with respect to cantilevers length is at the settled region of the time interval. The period selected from this interval is divided into 4 segments, it is assumed that deflections of *I* and *IV* segments are equal in magnitude as well as *II* is equal to *III*, they only differ in sign. The same methodic was used for other two cantilevers that were excited at their second resonant frequency of 534 Hz. Fig. 6 represents distribution of normal strains in horizontal direction in upper cantilever edge with respect to cantilevers length in meters for given interval of time.

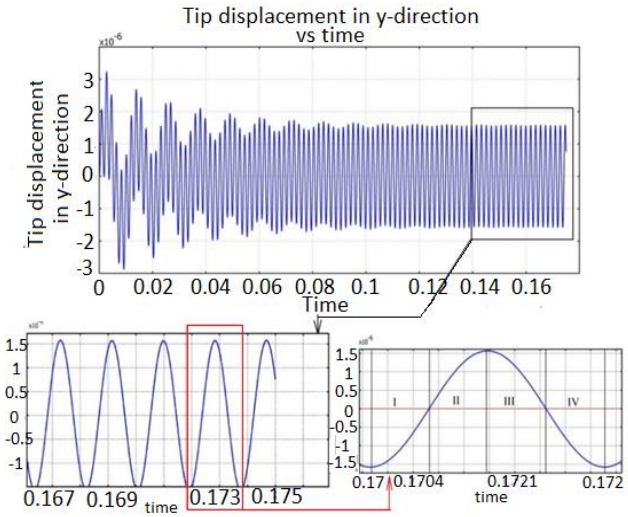

Fig. 5 Harvesters tip amplitude in the transverse direction: a) versus time; b) time interval selected for further investigation of normal deflections; c) time period 4 segments

The number of curves represents the number of time steps that the time interval was divided to. From Fig. 6 it can be seen that positive strains appear from 0 m to a = 0.0189 m of the cantilever with strains curve bounded area A^+, while negative – from b = 0.42 m to 0.1 m with strains curve bounded area A^-. Bounded areas A^+ and A^- are computed by integration a strain-displacement equation:

$$A_{t_i}^+ = \int_0^a \frac{\partial u}{\partial x} dx; \tag{5}$$

$$A_{t_i}^- = \int_b^l \frac{\partial u}{\partial x} dx, \tag{6}$$

where $A_{t_i}^+$ is the normal strain of positive sign in transverse direction of the cantilever at time step and $A_{t_i}^-$ is the normal strain of negative sign in transverse direction of the cantilever at time step t_i. It is seen that this problem can be reduced to finding the area of the region bounded above by the graph of a function $\frac{\partial u}{\partial x}$, where u – displacement in horizontal direction, x – horizontal axis. Bounded below by the x-axis (cantilevers length), bounded to the left by the vertical line a = 0.0189, and to the right by the vertical line b = 0.0416. As each different curve represents different point of time area bounded by each curve has to be calculated $A = A^- + A^+$ where $A^+ = A_{t1}^+ + A_{t2}^+ + \ldots + A_{tn}^+$ and $A^- = A_{t1}^- + A_{t2}^- + \ldots + A_{tn}^-$ as shown in Fig. 5, where A_{t1}^+ is normal strain of positive sign at time step 1, and A^+ is total sum normal strain for given sign for each of time steps, where n number of time steps. *A* represents the total sum of both positive and negative normal strain. The left side of the region of uncertainty at which the effective normal strain will be added to A^+ area from Fig. 5. It is calculated by subtracting the area bounded by normal strain curves in the negative part of the graph from area bounded by curves in the positive part of the graph: A_L^+ - A_L^- from 0.0196 m to 0.024039 m. Where, A_L^+ is the sum of positive normal strain at each time step in the left side of the region and A_L^- - negative.

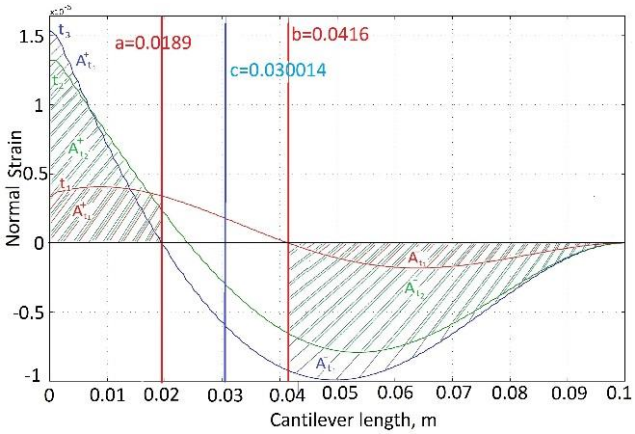

Fig. 6 Normal strain versus length of the cantilever. Vertical lines *a* and *b* represents boundaries of the region of uncertainty, while *c* – geometric middle of the region of uncertainty

The right side of the region of uncertainty at which the gain will be added to A^- area from Fig. 5. It is calculated by subtracting the area bounded by normal strain curves in the opposite part of the graph from area bounded by curves in the negative part of the graph: A_R^- - A_R^+ from 0.024039 m to 0.0416 m, where, A_R^+ is the sum of positive normal strain at each time step in the right side of the region and A_R^- - negative. Optimal segmentation was found to be at 0.024039 m by the method of semi-crossing [5].

Total normal strain in transverse direction $\sum A$ is found as $\sum A = A^+ + A^- + A_L + A_R$. It represents the total normal strain per given period of time at one face of the cantilever. The effective area calculation is done for both optimal and suboptimal segmentation of the cantilever to make the comparison of the gain of the segmentation as

A_{opt} versus A_{Sub}. For the investigated cantilever harvesters n = 18 time step per 1/4 period are used for more precise results. The optimal segmentation and gain was found for a rectangular cantilever at its second resonant frequency $\omega_2^{rect} = 514$ Hz, optimal design cantilevers at its second and third resonant frequencies $\omega_2^{opt} = 534$ Hz. The later sections of the work presents the results of calculation for different cantilever setups at their resonant frequencies.

3. Results

The graphic representation of calculation position of optimal segmentation of three cantilevers is shown in Fig. 7. From Fig. 7, a it can be observed that in the rectangular cantilever the optimal segmentation line is shifted quite far from the geometric center of the region of uncertainty, while in Fig. 7, b and c where the optimal shape cantilever are shown the optimal segmentation line has been shifted by very small amount. It is also obvious that normal strain curves are quite symmetric with respect to the center of the region while in the rectangular cantilever the symmetry is lost. Correlation between symmetry of the normal strain curves and optimal segmentation can be outlined. Finding optimal segmentation allowed the calculations of total normal strain gain with optimal segmentation versus sub-optimal segmentation. The normal strain curves were integrated to find the total normal strain at each step of time for optimal and sub-optimal segmentation. Total normal strain calculation method for constant sign sections of the cantilevers can be seen in Fig. 7 for each cantilever, where A_{t_i} is the total normal strain for given step of time t_i of positive or negative sign. The gain calculation results are given in Table 2. From this table it can be seen that the biggest gain was found in the rectangular cantilever, where the segmentation shift was also the greatest and distribution of normal strain was the least symmetric with respect to the center of uncertainty.

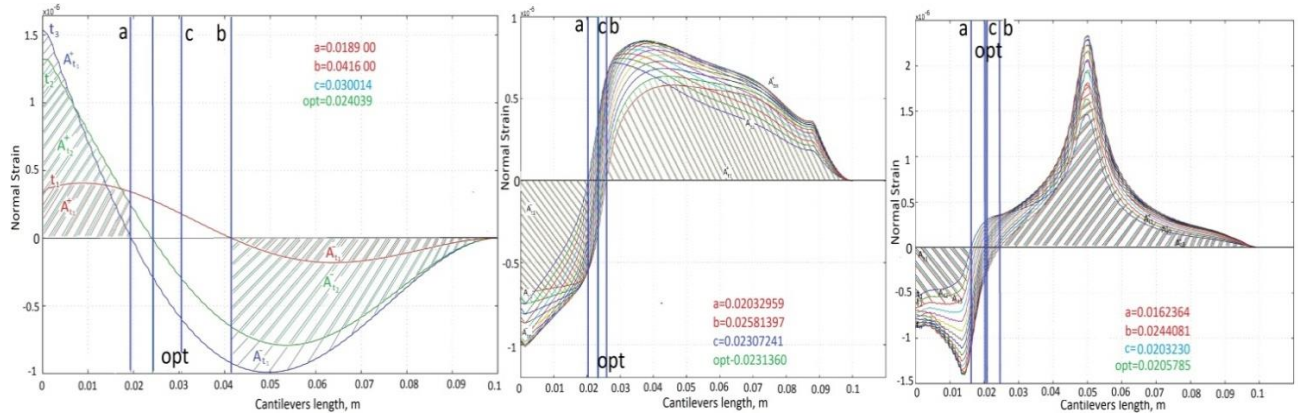

a b c

Fig. 7 Normal strain versus length: a) of the rectangular bimorph cantilever excited at its second resonant frequency of 541 Hz; b) of the optimal shape cantilever of second mode and c) of the optimal shape cantilever of third mode are excited at their second resonant frequency of 534 Hz

Table 2

Total normal strain gain calculation results for three types of cantilever energy harvesters

Cantilever type	Segmentation position along cantilever, m	Total strain in x-direction	Region of uncertainty gain, %			Total Gain, %
			Normal strain in region of uncertainty versus total normal strain, %	Normal strain in region of uncertainty	Gain in region of uncertainty, %	
Rectangular						
Optimal	*Opt* = 0.024039	0.762948	14.59	0.111301	+37.6%	+4.15%
Sub-Optimal	*C* = 0.030014	0.732532	11.01	0.080885		
OPTII						
Optimal	*Opt* = 0.023136	0.891478	1.03	0.00918	+0.128%	+0.0013%
Sub-Optimal	*C* = 0.023072	0.891466	1.02	0.00917		
OPTIII						
Optimal	*Opt* = 0.020579	0.983534	4.19	0.03751	+12.5%	+0.0425%
Sub-Optimal	*C* = 0.020323	0.979361	3.42	0.03333		

On the other hand the gain in optimal shape cantilevers is very small, only 0.0013% in optimal shape cantilever for the second resonant frequency and 0.0415% for optimal shape cantilever for third resonant frequency. From Table 2 it can be seen that region of uncertainty contained large proportion of total normal strain of bimorph rectangular cantilever, optimization of this region gained 37.6% more usable strain in this region and due to its large proportion (14.59% of total normal strain output) in total normal strain the total gain was also big.

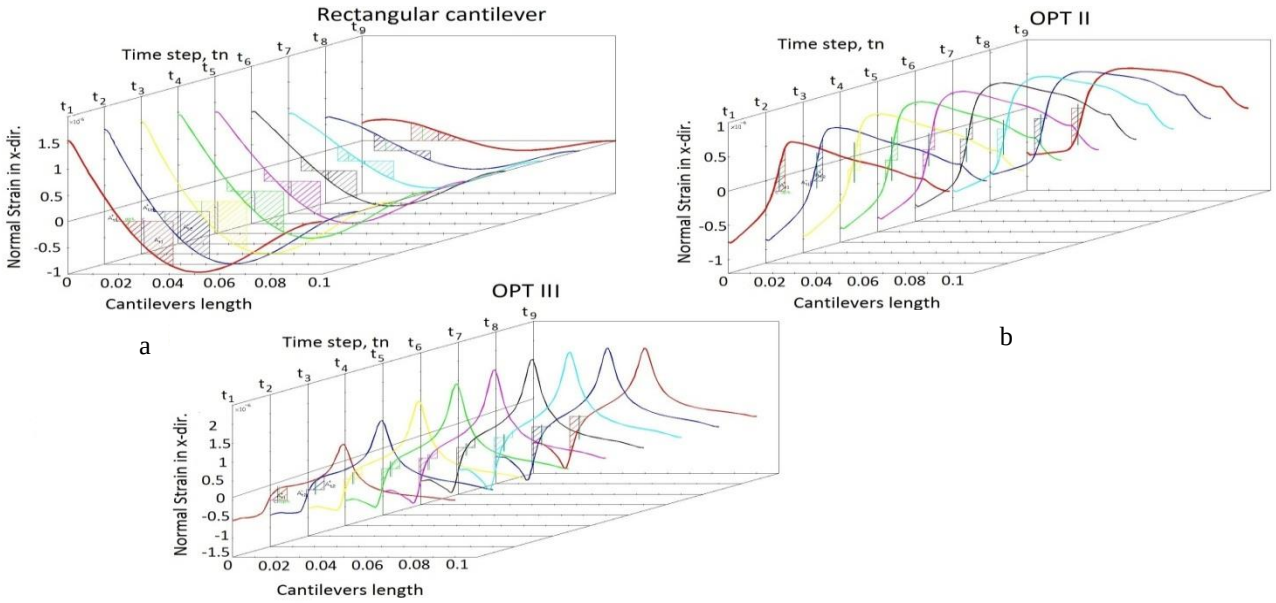

Fig. 8 Spread graphic of the normal strain versus length of the cantilever excited at the second transverse resonant frequency at time step t_i: a) rectangular cantilever b) optimal shape cantilever of the second mode c) optimal shape cantilever of the third mode

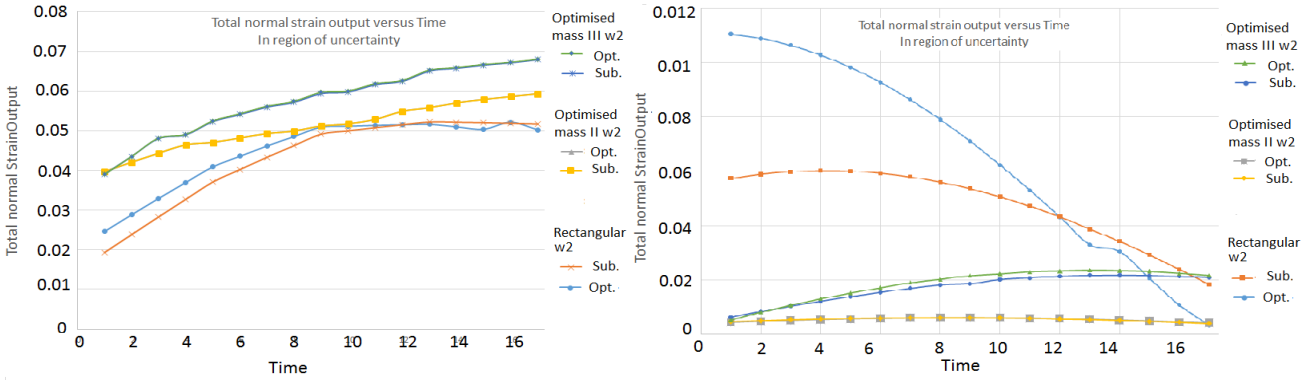

Fig. 9 Total normal strain output versus time step for the three cantilever setups at optimal and suboptimal segmentations: a) for all cantilever length; b) in region of uncertainty.

From Table 2 it also can be observed that optimal shape cantilevers had quite small regions of uncertainty and optimization did not make big effect on total normal strain output. The proportions of the region of uncertainty versus total normal strain outputs of the cantilevers were only 1% and 4% for optimal shape cantilevers respectively so naturally optimization of this region gave small increase in terms of total normal strain output. Fig. 8 illustrates the spread graphic of the total normal strain versus length of the cantilever at time step t_i. Total normal strain output versus time step can be seen in Fig. 9. Here Fig. 9, a represents comparison of total normal strain outputs of all three cantilevers. From here it can be seen that the biggest energy output has been reached in optimal shape cantilever of the third mode excited by the second resonant frequency. The smallest total normal strain or equivalent energy output has been registered in rectangular cantilever through the difference between optimal and sub-optimal segmentation outputs was the greatest in this bimorph cantilever setup. From Fig. 9 it can be seen that the widest region of uncertainty with biggest normal strain is observed in rectangular cantilever. Fig. 9 indicates that for the optimal shape cantilevers optimal and sub-optimal segmentation total normal strain output curves overlap (only 4 curves can be seen instead of 6). From Fig. 8, a it can be seen that only the rectangular bimorph cantilever shows large difference between optimal and suboptimal segmentation. Optimal shape bimorph cantilever curves overlap in optimal and sub-optimal segmentation revealing very little difference between optimal and sub-optimal cantilever performance under the same conditions. Fig. 9, b demonstrates that the difference between optimal and sub-optimal segmentation for rectangular cantilever is even bigger, as well as for optimal shape cantilever for the third resonant frequency excited by the second resonant frequency, though in this case the ratio of total normal strain output in region of uncertainty versus total normal strain output for the whole cantilever is very small. The results show that due to optimal shape of the cantilevers the normal strain distribution is localized in certain nodes of the cantilever and thus the ineffective loss of usable normal strain along cantilever is eliminated or minimized. This is seen from Fig. 8, b

where rectangular cantilever demonstrates large difference between optimal and sub-optimal segmentation in region of uncertainty, while the optimal shape cantilevers show very small difference between optimal and sub-optimal segmentation. Fig. 10 Represents the results of the optimal segmentation of the cantilevers. Here Fig. 10 schematic representation can be seen of three cantilevers with optimal segmentation of piezoelectric layers and directions of polarization for these layers when they are excited by the second mode of transverse vibrations.

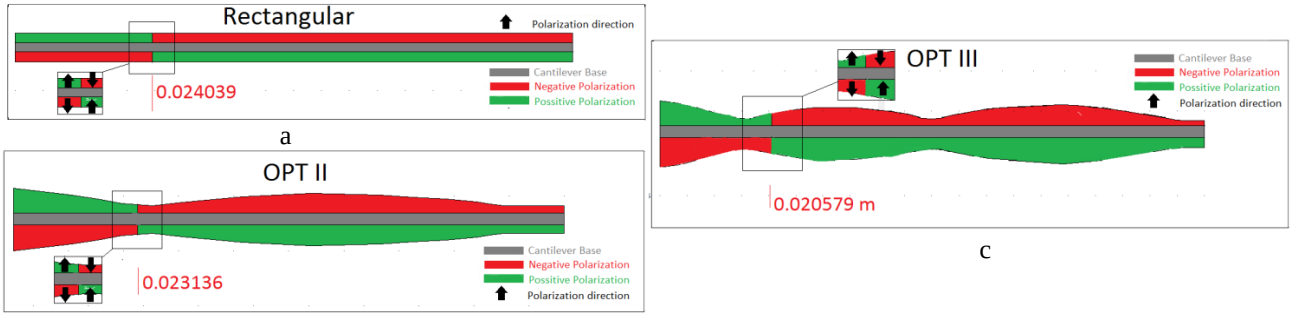

Fig. 10 Schematic representation of three optimal segmentation cantilever setups with directions of polarization for piezoelectric material: a) rectangular cantilever b) optimal shape cantilever of the second mode c) optimal shape cantilever of the third mode

4. Conclusions

Optimal segmentation along the length of the cantilever was calculated for each cantilever setup. Optimal segmentation position: for rectangular cantilever is 0.024039 m; for the optimally-shaped cantilever of the second mode of transverse vibrations - 0.023136 m; for the optimally-shaped cantilever of the third mode of transverse vibrations - 0.020579 m.

Total normal strain amount of sub-optimal configuration of the bimorph rectangular sub-optimal segmentation cantilever - 0.732532, of optimal segmentation 0.762948. For the optimally-shaped cantilever for the second eigen-frequency – suboptimal 0.891466, optimal 0.891478 and, for optimally-shaped cantilever for the third eigen-frequency suboptimal 0.97936, optimal 0.98353.

Total gain of optimal segmentation cantilever versus sub-optimal was found to be 4.15%, and 0.00013% and 0.0425% for the optimally-shaped cantilevers for the second and the third eigen-frequencies respectively.

Optimally-shaped cantilevers had narrower region of uncertainty and smaller ratio of total normal strain amount in region of uncertainty versus rectangular cantilever. Total normal strain in bimorph rectangular cantilever was smaller if compared to the optimized cantilevers due to larger losses of strain due to wide region of uncertainty.

Acknowledgments

This research was funded by a grant (No. MIP-060/2012) received from the Research Council of Lithuania.

References

1. **Adnan Harb** 2011. Energy harvesting: State-of-the-art, Department of Electrical Engineering, UAE University, 17555 Al Ain, United Arab Emirates, Renewable Energy 36: 2641-2654.
2. **Glynne, J.P.; Beeby, S.P.; White, N.M.** 2001. Towards a piezoelectric vibration powered microgenerator, IEE Proc. Sci. Meas. Technol. 148(2): 68-72. http://dx.doi.org/10.1049/ip-smt:20010323.
3. **Beeby, S. P.; Tudor, M.J.; White, N.M.** 2006. Energy harvesting vibration sources for microsystems applications, IEE Proc. Sci. Meas. Technol. 17: R175-R195. http://dx.doi.org/10.1088/0957-0233/17/12/R01.
4. **Dauksevicius, R.; Kulvietis, G.; Ostasevicius, V.; Gaidys, R.; Milasauskaite, I.** 2011. Multiphysical modeling of a contact-type piezotransducer for the analysis of micro-energy harvesting from ambient vibrations, J. of Vibroengineering 13(2): 342-351.
5. **Dauksevicius, R.; Kulvietis, G.; Ostasevicius, V.; Milasauskaite, I.** 2010. Finite element analysis of piezoelectric microgenerator - towards optimal configuration; EUROSENSORS XXIV Conference Book Series: Procedia Engineering 5: 1312-1315.
6. **Ostasevicius, V.; Gaidys, R.; Dauksevicius, R.** 2009. Numerical Analysis of dynamic effects of a nonlinear vibro-impact process for enhancing the reliability of contact-type MEMS devices, Sensors 9**(**12**):** 10201-10216. http://dx.doi.org/10.3390/s91210201.
7. **Minazara, E.; Vasic, D.; Costa, F.** 2008. Piezoelectric generator harvesting bike vibrations energy to supply portable devices, In Proceedings of International Conference on Renewable Energies and Power Quality (ICREPQ'08), Santander, Spain, 12-14.
8. **Amirtharajah, R.; Chandrakasan, A., P.** 1998. Self-powered signal processing using vibration-based power generation, IEEE J. Solid State Circuits 33(5): 687-695. http://dx.doi.org/10.1109/4.668982.

D. Žižys, R. Gaidys, R. Daukševičius, V. Ostaševičius

NORMALINIŲ DEFORMACIJŲ PASISKIRSTYMO OPTIMALIOS FORMOS BIMORFINĖSE GEMBĖSE, ŽADINAMOSE ANTRUOJU REZONANSINIU DAŽNIU, TYRIMAS IR PJEZOELEKTRINIŲ SLUOKSNIŲ SEGMENTAVIMAS

R e z i u m ė

Straipsnio tikslas – ištirti normalinių deformacijų pasiskirstymą išilgai gembės, žadinamos antruoju rezonansiniu skersinių virpesių dažniu. Buvo tiriamos trijų skirtingų formų gembės: stačiakampė gembė, optimalios formos gembė, žadinama antruoju rezonansiniu skersinių virpesių dažniu, ir optimalios formos gembė, žadinama trečiuoju rezonansiniu skersinių virpesių dažniu. Atlikus tyrimą apskaičiuotos šių gembių optimalaus segmentavimo vietos, kuriose tempimo deformacijas keičia gniuždymo deformacijos ir atvirkščiai. Nustatyta, kad optimalios formos gembių kintamų deformacijų zona yra siauresnė, taip pat joje yra mažiau deformacijų, palyginti su stačiakampe gembe. Stačiakampėje gembėje naudingųjų deformacijų būna mažiau nei optimalių formų gembėse. To priežastis – plati gembės zona, kurioje deformacijos keičia ženklą, o tai sąlygoja deformacijų kiekio nuostolius.

D. Žižys, R. Gaidys, R. Daukševičius, V. Ostaševičius

SEGMENTATION OF PIEZOELECTRIC LAYERS BASED ON THE NUMERICAL STUDY OF NORMAL STRAIN DISTRIBUTIONS IN BIMORPH CANTILEVERS VIBRATING IN THE SECOND TRANSVERSE MODE

S u m m a r y

The objective of this paper is to study normal strain distribution along the length of a bimorph piezoelectric cantilever when it is excited at the second mode of transverse vibrations. The analysis was performed with three cantilevers of different shapes: rectangular, optimally-shaped with respect to the second transverse mode and optimally-shaped with respect to the third transverse mode of the rectangular cantilever. The eigen-frequencies of the vibration modes have the same value for all the cantilevers. Numerical study provided optimal segmentation of the piezoelectric layer boundaries, where tensile deformations change into compression ones and vice versa. It is concluded that the optimally-shaped cantilevers had narrower region of uncertainty and smaller ratio of total normal strain amount in the region of uncertainty versus rectangular cantilever. Total normal strain in the bimorph rectangular cantilever was smaller if compared to the optimized cantilevers due to larger losses of strain due to wide region of uncertainty.

Keywords: piezoelectric energy harvesting, total normal strain, optimal shape cantilever.

Received December 03, 2012
Accepted August 21, 2013